

Experimental Demonstration of the Collisionless Plasmoid Instability below the Ion Kinetic Scale during Magnetic Reconnection

J. Olson, J. Egedal, S. Greess, R. Myers, M. Clark, D. Endrizzi, K. Flanagan, J. Milhone, E. Peterson, J. Wallace, D. Weisberg, and C. B. Forest

Department of Physics, University of Wisconsin-Madison, 1150 University Avenue, Madison, Wisconsin 53706, USA

(Received 28 February 2016; published 20 June 2016)

The spontaneous formation of magnetic islands is observed in driven, antiparallel magnetic reconnection on the Terrestrial Reconnection Experiment. We here provide direct experimental evidence that the plasmoid instability is active at the electron scale inside the ion diffusion region in a low collisional regime. The experiments show the island formation occurs at a smaller system size than predicted by extended magnetohydrodynamics or fully collisionless simulations. This more effective seeding of magnetic islands emphasizes their importance to reconnection in naturally occurring 3D plasmas.

DOI: 10.1103/PhysRevLett.116.255001

Magnetic reconnection is defined as the rearrangement of magnetic field line topology in the presence of a plasma, permitting magnetic stress to be released in often explosive events [1]. Although the details of how reconnection occurs in nature are still not fully understood, reconnection is believed to drive a range of phenomena including solar flares [2] and magnetic substorms in the Earth's magnetosphere [3]. Resistive fluid models (resistive magnetohydrodynamics) show that as the resistivity of the plasma is decreased to a sufficiently low value reconnection will transition from a slow regime characterized by Sweet-Parker reconnection [4,5] into a much faster regime characterized by the formation of magnetic islands [6], also called plasmoids. Based on work using primarily 2D fluid models, it has been theorized that the island instability is responsible for the onset of solar flares [7]. Furthermore, the subsequent coalescence of magnetic islands may provide an effective mechanism for the generation of superthermal electrons [8]. From theory, it is expected that the magnetic island instability becomes effective when reconnection current layers become much larger than the length scales associated with the ion dynamics. In contrast, in this Letter we provide direct experimental evidence that the magnetic island instability is active when the current layer is at length scales associated with the electrons.

The plasma regimes where plasmoids (or multiple X -line reconnection) are expected can be laid out using a phase diagram developed by Daughton and Roytershteyn [9] as a function of the Lundquist number S and the normalized system size L/λ , where $S = \mu_0 L_{CS} V_A / \eta$, L_{CS} is the size of the current sheet, V_A is the Alfvén speed evaluated using the reconnection magnetic field, and η is the plasma resistivity. Here, $\lambda = \min(d_i, \rho_s)$ characterizes the ion dynamics length scale as the smaller of the ion skin depth $d_i = c/\omega_{pi}$, or the ion sound Larmor radius $\rho_s = [m_i(T_i + T_e)]^{1/2}/eB$. Figure 1 displays this phase diagram, summarizing the current

theoretical and numerical understanding of reconnection dynamics.

Collisional reconnection becomes susceptible to magnetic island formation above a critical Lundquist number $S_{crit} = 10^4$ [10], marked by the horizontal green line. As the collisionality decreases and the Sweet-Parker current layer width approaches the appropriate ion kinetic scale [11,12] a transition to collisionless reconnection occurs, dominated by kinetic effects. This regime is indicated above the solid black line [13]. Though there is no analytic theory, large scale particle-in-cell simulations indicate the presence of multiple X lines above a critical system size $L_{crit}/\lambda \sim 40$,

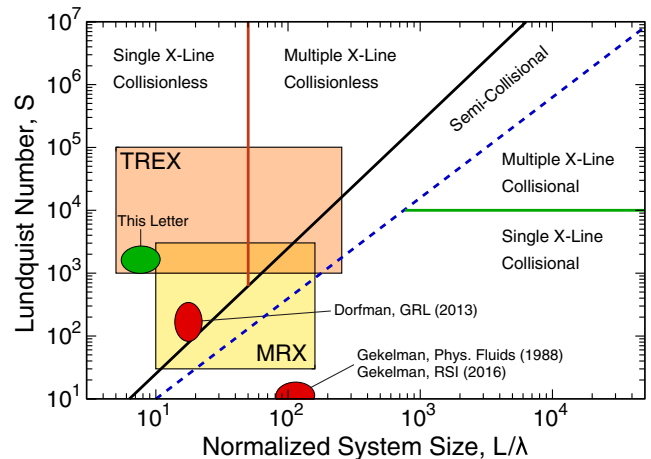


FIG. 1. Theoretical phase diagram indicating different regimes of reconnection where multiple X lines separated by plasmoids are expected for both collisional and collisionless reconnection as a function of the Lundquist number and the normalized system size. The shaded regions map out accessible plasma parameters of both TREX and MRX. Other notable results from tearing experiments are marked with red ovals. The results presented here fall into the collisionless regime where multiple X lines are not expected from theory.

the vertical orange line, during collisionless magnetic reconnection [14,15].

The existence of magnetic islands is well documented through *in situ* observations [16–18] under fully collisionless conditions in the Earth’s magnetotail and can also be observed during solar flare events [19,20]. Transient reconnection can also lead to small scale magnetic substructures at secondary reconnection sites many d_i from the central X line [21,22]. In laboratory experiments, direct observation of secondary magnetic islands has been limited due to the inability to reach the critical parameters predicted by theory. The recent inclusion of a semicollisional region [23] likely accounts for some of the islands observed in the Magnetic Reconnection eXperiment (MRX) [24]. Additionally, studies of electron layer tearing have been done on linear experimental devices at large guide field and small reconnection magnetic field values, placing these experiments in a low- S and high- L/λ regime [25,26]. In contrast, the magnetic islands discussed here are sufficiently collisionless and develop at such small normalized current layer length scales that their occurrence is unexpected based on theory.

The new Terrestrial Reconnection eXperiment (TRES) is in operation at the Wisconsin Plasma Astrophysics Laboratory [27]. Figure 2(a) shows a 3D rendering of the 3 m diameter spherical vacuum vessel with the TRES hardware implemented. A toroidal cross section of the vessel is shown in Fig. 2(b) in which the defined RZ plane, with the positive toroidal direction pointing out of the plane, is used for all future plots. For the present experiments, helium plasmas are initiated by biasing LaB_6 electrodes at the edge of the vessel. The basic configuration includes a steady, axial magnetic field from an external Helmholtz coil and no applied guide field in the toroidal direction. In addition, two 2 m diameter coils are installed inside the vacuum vessel. During the initial phase of coil energization, new magnetic flux surfaces expand rapidly away from the coils and a reconnection current sheet forms where the oppositely directed magnetic flux pushes against the Helmholtz field. As the current in the internal coils is rapidly increased, the reconnection layer migrates toward the center of the device. The resulting vacuum field is sketched in Fig. 2(b). The setup is nominally 2D due to the axisymmetry of the device about the Z axis, but 3D effects can develop freely during the reconnection process, as in any experiment. The facility allows for experimentation with plasmas in a parameter regime where collisions do not influence the momentum balance between the electrons and ions.

The main diagnostic is a magnetic flux array outlined in Fig. 2. Similar to previous reconnection experiments [28], the flux array measures the magnetic flux function Ψ on a grid of 16×9 simple Faraday pickup loops. The grid has 16 positions from 0 to 80 cm in R and nine positions covering -30 to 50 cm in Z , where the widths of each loop

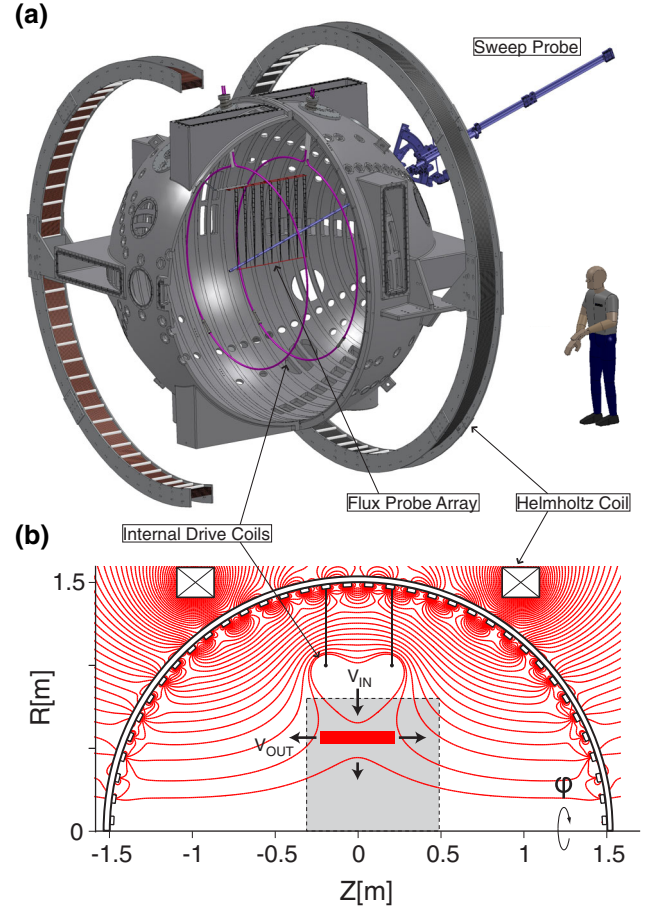


FIG. 2. (a) Schematic of the Wisconsin Plasma Astrophysics Laboratory in the TRES configuration, including the magnetic diagnostic suite. To drive reconnection, the internal coils are pulsed opposite the steady state field provided by the external Helmholtz coil. (b) Calculated vacuum magnetic fields during a pulse overlaid with an illustration of the plasma inflows and outflows as the reconnection current layer propagates toward the center of the vessel. The shaded gray box indicates the areal coverage of the array of 144 magnetic flux probes.

are proportional to R . Because of this symmetry, the loops directly measure $\dot{\Psi} = \dot{\Psi}(R, Z) - \dot{\Psi}(R_0, Z_0) = \int_{R_0}^R R' B_Z(R', Z) dR'$, where $\dot{\Psi}(R_0, Z_0) = 0$ by definition. Ψ can then be numerically integrated to get the full magnetic flux function. In addition, a linear array of ten three-axis magnetic probes measures magnetic signals in a separate toroidal plane, offset by 15° . Values for the plasma density and temperature are measured by a probe with 16 closely spaced Langmuir tips individually biased from ± 120 V, allowing the full IV characteristics to be obtained with a 2 MHz resolution at the location of the probe.

For the event presented in Fig. 3, the reconnection drive was applied at $t = 0$ s and the reconnection current layer was observed at $R \sim 0.45$ m for $t \approx 145 \mu\text{s}$. Based on the measurement of Ψ , key profiles characterizing the reconnection process are readily computed, including the B_Z magnetic field and the out-of-plane current density J_ϕ

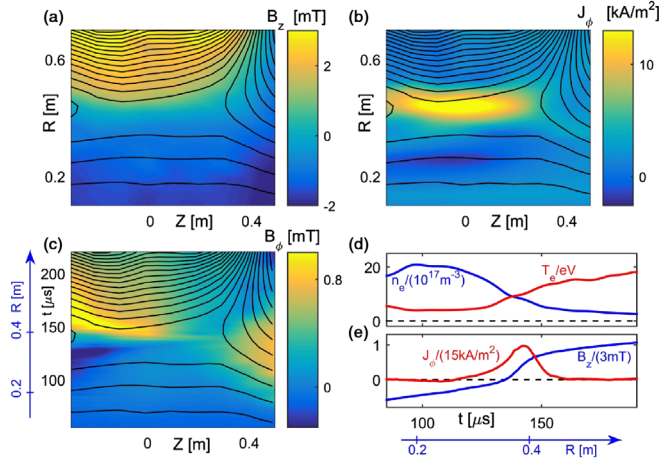


FIG. 3. Profiles of (a) the reconnecting magnetic field B_Z and (b) the out-of-plane current density J_ϕ measured by the flux array. The contour lines of constant magnetic flux Ψ show the in-plane projection of magnetic field lines. (c) The out-of-plane Hall magnetic field B_ϕ measured by the linear magnetic array. (d) Profiles of the electron density and temperature measured by a multiple Langmuir probe array. The temporal axis in (c) and (d) is converted to a spatial axis knowing the velocity of the current layer, $V_R \sim -4$ km/s, as it flows passed each probe. (e) Profiles at $Z = 0$ m of J_ϕ and B_Z inferred from (a) and (b).

shown in Figs. 3(a) and 3(b). The contours of Ψ provide the instantaneous geometry of the in-plane magnetic field lines. The current layer in Fig. 3(b) separates two inflow regions of oppositely directed magnetic fields. We note how the TREX configuration allows for long current layers to form without the reconnection exhausts being obstructed by downstream obstacles and associated pressure buildup influencing the reconnection rate [29].

The quadrupolar Hall magnetic fields, transverse to the reconnecting plane, are clearly present in Fig. 3(c) and serve as a signature of two-fluid reconnection [30]. They are generated by the Hall currents resulting when the ion and electron fluids decouple inside the ion diffusion region, which has a characteristic width of an ion skin depth. The Hall fields have been observed *in situ* by spacecraft [31] and previous laboratory experiments in MRX [32].

Similar to configurations in the solar wind [33] and in the dayside magnetopause [34], the reconnection layer in TREX plasmas exhibits strong asymmetries in kinetic profiles across the current sheet. Using the temperature probe described earlier, time profiles of number density n_e and electron temperature T_e at $R \sim 0.45$ m and $Z \sim 0.0$ m were obtained as displayed in Fig. 3(d). In addition, the profiles of B_Z and J_ϕ in Fig. 3(e) were inferred from the flux array data at the location of the temperature probe. Together, these profiles show asymmetric reconnection with an enhanced plasma density $n_1 \sim 2 \times 10^{18} \text{ m}^{-3}$ on the low-field side of the reconnection layer, $B_{Z1} \sim -1.5$ mT, compared to $n_2 \sim 4 \times 10^{17} \text{ m}^{-3}$ on the high-field side, $B_{Z2} \sim 3$ mT. We note that the asymmetries in the

profile of B_ϕ in Fig. 3(c) are consistent with the expectations for asymmetric reconnection [35] where the Hall fields are most pronounced on the side of the current layer with the largest B_Z .

The out-of-plane inductive electric field E_ϕ is also easily computed from the magnetic flux function. The value of E_ϕ at the X point is taken as the reconnection electric field E_{rec} and characterizes the fast reconnection rate on TREX. In the absence of magnetic island dynamics, the observed reconnection electric field is approximately $E_{\text{rec}} \sim 15$ V/m. Following the formalism of previous experimental investigations we may then infer an effective resistivity $\eta^* = E_{\text{rec}}/J_\phi = (15 \text{ V/m})/(15 \text{ kA/m}^2) \sim 10^{-3} \Omega\text{m}$. In comparison, for the observed electron temperature of $T_e \sim 10$ eV within the current layer, the transverse Spitzer resistivity is $\eta_{\text{sp}} \sim 8.8 \times 10^{-6} \Omega\text{m}$. Thus, the ratio of the effective resistivity to the Spitzer value ($\eta^*/\eta_{\text{sp}} \sim 10^2$) is larger by about a factor of 10 compared to those observed in MRX [11]. We also note the reconnection electric field is well above the Dreicer limit $E_D = (m_e T_e)^{1/2} v_{ei}/e \sim 2.5$ V/m, where the acceleration of the electrons outweighs the collisional drag, confirming that TREX operates deeper in the collisionless regime, as indicated in Fig. 1.

The reconnection geometry can be characterized by a set of dimensionless parameters appropriate to asymmetric reconnection [36]. We use the electron density $n_e \sim 10^{18} \text{ m}^{-3}$ observed in the center of the current layer to evaluate the typical electron and ion skin depths, $d_e \sim 0.006$ m and $d_i \sim 0.54$ m. Thus, the size of the experiment is about $L_{\text{exp}} \sim 5d_i$, while the half length of the current layer is $L_j \sim 0.7d_i$. Normalized to the electron length, we note that $L_j/d_e \sim 90$ is similar to that observed in kinetic simulations. Meanwhile, the observed normalized half width of the current layer $\delta_j/d_e \sim 8$ is wider than what is observed in kinetic simulations, but similar to other reconnection experiments [37]. To evaluate the relevant Alfvén speed for the asymmetric configuration we follow the convention of Ref. [36], $V_{A,\text{asym}} = \{B_1 B_2 (B_1 + B_2) / [\mu_0 m_i (n_1 B_2 + n_2 B_1)]\}^{(1/2)} \sim 20$ km/s. We may then calculate the Lundquist number $S = 2L_j \mu_0 V_{A,\text{asym}} / \eta_{\text{sp}} \sim 10^3$, where we have used $2L_j \sim 0.7$ m for the full length of the current layer. The phase diagram in Fig. 1 is updated with the measured values from these experiments. Furthermore, the typical E_{rec} is larger than the expected Cassak-Shay reconnection electric field [36], $E_{\text{rec}}/E_{\text{CS}} \sim 3$, where $E_{\text{CS}} = (2\delta_j/L_j) V_{A,\text{asym}} B_1 B_2 / (B_1 + B_2) \sim 6$ V/m.

Of particular interest from the recent experiments is the spontaneous formation and ejection of often multiple magnetic islands from within a single reconnection layer. As an example, Figs. 4(a)–4(f) provide snapshots of the plasma current density overlaid with contours of constant Ψ during one of these events. Initially, the reconnection current layer is formed as in Fig. 3(b). Figures 4(a) and 4(b) then show the reconnection of the two X lines within the current sheet forming the first plasmoid, where the

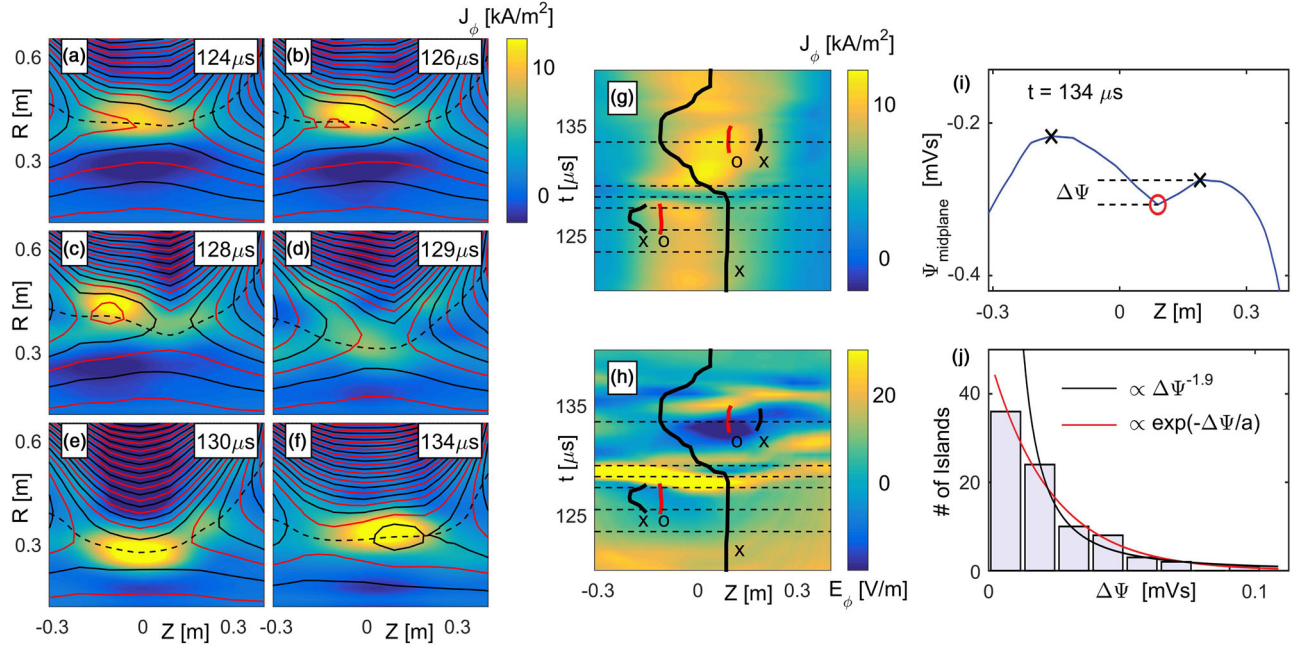


FIG. 4. (a)–(f) Measured 2D profiles of the out-of-plane current density J_ϕ and magnetic flux contours; $\Psi = \text{const}$. The occurrence of separate plasmoids is clearly visible for $t = 128 \mu\text{s}$ and $t = 134 \mu\text{s}$. The dashed lines indicate the midplane where $B_Z = 0$. Here $1 \mu\text{s} \times f_{ce} \sim 50$, where the electron gyrofrequency f_{ce} is evaluated with the average reconnection magnetic field. (g), (h) Time evolution of J_ϕ and the inductive electric field E_ϕ evaluated at the midplane as a function of Z and t . The dashed lines correspond to the midplanes from frames (a)–(f). The O and X points are marked with red and black lines, respectively. (i) Magnetic flux Ψ observed at the midplane for $t = 134 \mu\text{s}$. The X points are located as local maxima, while the O points coincide with the local minimum. $\Delta\Psi$ provides a measure for the size of the islands. (j) Statistical study of the size of the magnetic islands. Islands from 85 discharges are binned according to their size measured by $\Delta\Psi$ of panel (i). The data are consistent with both exponential and power-law dependencies for the island occurrence rate as a function of the island size.

contours in Fig. 4(c) make a closed loop $\sim 0.1d_i$ wide. Because of the magnetic tension, the plasmoid is subsequently ejected, corresponding to a sharp decline in the current density. After the current density recovers and the layer continues to reconnect, a second plasmoid is formed and then ejected in a similar manner. With $S \sim 1000$ and $L_j/d_i \sim 1$ it should be expected that our experiment will fall deeply into a regime of single X -line, collisionless reconnection, and yet plasmoids are clearly present.

The observed island behavior shows explosive and dynamic modifications to the reconnection process. To provide an overview of how the island influences the reconnection process, Figs. 4(g) and 4(h) show J_ϕ and E_ϕ evaluated on the evolving midplane. The locations of X lines are shown as the solid black lines, while the locations of O points are marked as the solid red lines. The formation and ejection of magnetic islands are responsible for the strong variations in these profiles. First, as the islands grow and their currents increase, E_ϕ is reduced. Then, as the islands are ejected, large spikes in E_ϕ are observed. In fact, at $t \sim 128 \mu\text{s}$ when the island is ejected and the current in the layer declines, the inductive E_ϕ spikes from 10 to 50 V/m (saturating the applied color scale). The same pattern is observed again as the second island forms at a later time. A similar modification to the reconnection rate

due to island dynamics has been observed in simulations and demonstrates their importance to the overall dynamics of the reconnection process [14].

To standardize our analysis of multiple discharges, we characterize the plasma parameters observed at the middle of the current layers, where $B_Z = 0$, for each time point. To illustrate this, Fig. 4(i) displays Ψ evaluated as a function of Z along the midplane (indicated by the black dashed line) observed at $t = 134 \mu\text{s}$. The two X lines of Fig. 4(f) are identified as the local maxima of the curve in Fig. 4(i). The center of the island is characterized by the local minimum in Fig. 4(i) (marked by the red “ O ”). We define the difference in the flux between the O point and the X point of an island, $\Delta\Psi$, as a measure for the size of the island.

One or more magnetic islands are observed in 42 of the 85 similar discharges considered (a total of 81 islands are counted overall). To investigate the statistical properties of the magnetic island occurrence we analyze the island sizes observed in this ensemble of discharges. As shown in Fig. 4(j), the distribution of island sizes is well characterized by an exponential fit or, if the first data point is ignored due to the finite resolution of our magnetic diagnostics, a power-law fit.

In summary, we have observed electron scale magnetic islands being produced in a low collisional plasma for

current layers around one ion skin depth long, conflicting with the current understanding of plasmoid dynamics. Because magnetic islands are a fundamental ingredient in models for electron energization and increased reconnection dynamics, their high occurrence rate at these small scales suggests that magnetic islands may be seeded within larger systems, such as solar flares, much more effectively than suggested by present theoretical models.

We gratefully acknowledge the support by the National Science Foundation (NSF) Major Research Instrumentation program for construction of the facility. The TREX implementation was initiated with funds provided by the Physics Department of UW-Madison, and the research on reconnection is now supported by NSF and the U.S. Department of Energy.

-
- [1] E. Priest and T. Forbes, *Magnetic Reconnection* (Cambridge University Press, Cambridge, England, 2000).
- [2] J. Dungey, *Philos. Mag.* **44**, 725 (1953).
- [3] V. M. Vasyliunas, *Rev. Geophys.* **13**, 303 (1975).
- [4] P. A. Sweet, in *Electromagnetic Phenomena in Cosmical Physics*, IAU Symposium, Vol. 6, edited by B. Lehnert (Cambridge University Press, 1958), p. 123.
- [5] E. N. Parker, *J. Geophys. Res.* **62**, 509 (1957).
- [6] D. Biskamp, *Phys. Fluids* **29**, 1520 (1986).
- [7] K. Shibata and S. Tanuma, *Earth, Planets Space* **53**, 473 (2001).
- [8] J. F. Drake, M. Swisdak, H. Che, and M. A. Shay, *Nature (London)* **443**, 553 (2006).
- [9] W. Daughton and V. Roytershteyn, *Space Sci. Rev.* **172**, 271 (2012).
- [10] N. F. Loureiro, A. A. Schekochihin, and S. C. Cowley, *Phys. Plasmas* **14**, 100703 (2007).
- [11] M. Yamada, Y. Ren, H. Ji, J. Breslau, S. Gerhardt, R. Kulsrud, and A. Kuritsyn, *Phys. Plasmas* **13**, 052119 (2006).
- [12] J. Egedal, W. Fox, N. Katz, M. Porkolab, K. Reim, and E. Zhang, *Phys. Rev. Lett.* **98**, 015003 (2007).
- [13] H. Ji and W. Daughton, *Phys. Plasmas* **18**, 111207 (2011).
- [14] W. Daughton, J. Scudder, and H. Karimabadi, *Phys. Plasmas* **13**, 072101 (2006).
- [15] W. Daughton, V. Roytershteyn, H. Karimabadi, L. Yin, B. J. Albright, B. Bergen, and K. J. Bowers, *Nat. Phys.* **7**, 539 (2011).
- [16] L. J. Chen, A. Bhattacharjee, P. A. Puhl-Quinn, H. Yang, N. Bessho, S. Imada, S. Muehlbachler, P. W. Daly, B. Lefebvre, Y. Khotyaintsev, A. Vaivads, A. Fazakerley, and E. Georgescu, *Nat. Phys.* **4**, 19 (2008).
- [17] M. Øieroset, T. D. Phan, J. P. Eastwood, M. Fujimoto, W. Daughton, M. A. Shay, V. Angelopoulos, F. S. Mozer, J. P. McFadden, D. E. Larson, and K. H. Glassmeier, *Phys. Rev. Lett.* **107**, 165007 (2011).
- [18] H. S. Fu, J. B. Cao, Y. V. Khotyaintsev, M. I. Sitnov, A. Runov, S. Y. Fu, M. Hamrin, M. Andr, A. Retin, Y. D. Ma, H. Y. Lu, X. H. Wei, and S. Y. Huang, *Geophys. Res. Lett.* **40**, 6023 (2013).
- [19] N. Nishizuka, H. Takasaki, A. Asai, and K. Shibata, *Astrophys. J.* **711**, 1062 (2010).
- [20] S. Takasao, A. Asai, H. Isobe, and K. Shibata, *Astrophys. J.* **745**, L6 (2012).
- [21] M. I. Sitnov, M. Swisdak, and A. V. Divin, *J. Geophys. Res.* **114** (2009).
- [22] G. Lapenta, S. Markidis, M. V. Goldman, and D. L. Newman, *Nat. Phys.* **11**, 690 (2015).
- [23] N. F. Loureiro and D. A. Uzdensky, *Plasma Phys. Controlled Fusion* **58**, 014021 (2016).
- [24] S. Dorfman, H. Ji, M. Yamada, J. Yoo, E. Lawrence, C. Myers, and T. D. Tharp, *Geophys. Res. Lett.* **40**, 233 (2013).
- [25] W. Gekelman and H. Pfister, *Phys. Fluids* **31**, 217 (1988).
- [26] W. Gekelman, P. Pribyl, Z. Lucky, M. Drandell, D. Leneman, J. Maggs, S. Vincena, B. Van Compernelle, S. K. P. Tripathi, G. Morales, T. A. Carter, Y. Wang, and T. DeHaas, *Rev. Sci. Instrum.* **87**, 025105 (2016).
- [27] C. B. Forest *et al.*, *J. Plasma Phys.* **81**, 345810501 (2015).
- [28] A. Kesich, J. Bonde, J. Egedal, W. Fox, R. Goodwin, N. Katz, and A. Le, *Rev. Sci. Instrum.* **79**, 063505 (2008).
- [29] H. Ji, M. Yamada, S. Hsu, and R. Kulsrud, *Phys. Rev. Lett.* **80**, 3256 (1998).
- [30] B. U. Ö. Sonnerup, in *Magnetic Field Reconnection, in Solar System Plasma Physics*, Vol. 3, edited by L. T. Lanzerotti, C. F. Kennel, and E. N. Parker (North-Holland, New York, 1979), pp. 45–108.
- [31] A. L. Borg, M. Øieroset, T. D. Phan, F. S. Mozer, A. Pedersen, C. Mouikis, J. P. McFadden, C. Twitty, A. Balogh, and H. Rème, *Geophys. Res. Lett.* **32**, (2005).
- [32] Y. Ren, M. Yamada, S. Gerhardt, H. T. Ji, R. Kulsrud, and A. Kuritsyn, *Phys. Rev. Lett.* **95**, 055003 (2005).
- [33] J. T. Gosling, S. Eriksson, T. D. Phan, D. E. Larson, R. M. Skoug, and D. J. McComas, *Geophys. Res. Lett.* **34**, L06102 (2007).
- [34] T. D. Phan, M. A. Shay, J. T. Gosling, M. Fujimoto, J. F. Drake, G. Paschmann, M. Øieroset, J. P. Eastwood, and V. Angelopoulos, *Geophys. Res. Lett.* **40**, 4475 (2013).
- [35] J. Yoo, M. Yamada, H. Ji, J. Jara-Almonte, C. E. Myers, and L.-J. Chen, *Phys. Rev. Lett.* **113**, 095002 (2014).
- [36] P. A. Cassak and M. A. Shay, *Phys. Plasmas* **14**, 102114 (2007).
- [37] H. Ji, Y. Ren, M. Yamada, S. Dorfman, W. Daughton, and S. P. Gerhardt, *Geophys. Res. Lett.* **35**, L13106 (2008).